Influence of grain size, shape and compaction on georadar waves: examples of aeolian dunes

Julien Guillemoteau, Maksim Bano, Jean-Rémi Dujardin

Influence of grain size, shape and compaction on georadar waves: examples of aeolian dunes

Julien Guillemoteau, Maksim Bano and Jean-Remi Dujardin

Institut de Physique du Globe de Strasbourg & EOST, CNRS-UDS UMR 75–16, Strasbourg, France. E-mail: j.guillemoteau@unistra.fr (JG), maksim.bano@unistra.fr (MB)

SUMMARY

Many ground penetrating radar (GPR) profiles acquired in dry aeolian environment have shown good reflectivity inside present-day dunes. We show that the origin of this reflectivity is related to changes in grain size distribution, packing and/or grain shape in a sandy material. We integrate these three parameters into analytical models for bulk permittivity in order to predict the reflections and the velocity of GPR waves. We consider two GPR cross-sections acquired over aeolian dunes in the Chadian desert. The 2D migration of GPR data suggests that dunes contain different kinds of bounding surfaces. We discuss and model three kinds of reflections using reasonable geological hypothesis about aeolian sedimentation processes. The propagation and the reflection of radar waves are calculated using the 1D wavelet modelling method in spectral domain. The results of the forward modelling are in good accordance with real observed data.

Key words: Numerical solutions; Electrical properties; Electromagnetic theory; Ground penetrating radar.

INTRODUCTION

Ground penetrating radar (GPR) is a geophysical method based on electromagnetic wave (EM) propagation, which is sensitive to dielectric permittivity contrasts. The resolution of the GPR method depends on the velocity of EM waves and the frequency of the antennae used. Following the $\lambda/4$ criterion (Widess 1973; Jol 1995; Zeng 2009), it varies from 5 to 22 cm for frequencies of 200–500 MHz and velocities of 0.1–0.18 m/ns. At this scale of analysis, the dielectric constant of the effective medium is controlled by the volumetric fraction of each sub-material (rocks matrix, air and eventually water) that constitute rock. Therefore, one can say that the GPR response for rocks depends principally on the nature of its matrix, its porosity and its fluid saturation.

Many studies have shown that the GPR method can provide very detailed and continuous imaging of the internal structures of aeolian dunes and allow defining the relative chronology of sand deposition (Shenk *et al.* 1993; Bristow *et al.* 1996, 2005; Harari 1996; Bristow *et al.* 2000; Neal & Roberts 2001; Bano & Girard 2001; Adetunji *et al.* 2008). Other studies considering the physical properties of rocks have shown that the properties that might change are the grain size distribution (Otto 1938; Bagnold 1941; Barndorf-Nielsen *et al.* 1982; Watson 1986; Thomas 1988; Lancaster 1989; Wang *et al.* 2003), wind compaction (Bayard 1947; Hunter 1977) and/or the grain shape (Sen *et al.* 1981) in the case of sand/sandstone contact. These three structural parameters cause a macroscopic change of permittivity. Consequently, they should influence the GPR reflectivity within dry sand.

In this paper, we propose to explain these reflections by using a model of dry materials in which we can control the size, compaction and shape of the grain. First, we show how to incorporate granulometry data in the effective permittivity formulas for a mix of several grain sizes. Then, we propose a method to predict simultaneously both the porosity and permittivity of a bimodal mix of sand. For the third structural parameter, the grain shape, we simulate sand/sandstone contact by using the formula introduced by Sen *et al.* (1981). Finally, we compute the propagation and reflection of EM waves within a two-layer model that depends on these three parameters and compare the modelled GPR response with real data acquired over two aeolian sand dunes in the Chadian desert. We acknowledge that many other factors such as antenna radiation, ground coupling and scattering loss are not accounted for. In our analyses, these factors are assumed to change much more slowly than the effective permittivity in the case where reflections are observed in the data.

INFLUENCE OF GRAIN SIZE DISTRIBUTION ON THE PERMITTIVITY

The permittivity of rocks varies over a wide range of length scale. The GPR method is sensitive to permittivity contrasts for layers thicker than a few centimetres. However, the permittivity of each layer is controlled by smaller changes of permittivity occurring at the pore scale and/or by the ones caused by thinner laminations (around

1 cm of thickness) which might be due to the daily alternating wind power. At this scale of analysis, the quasi-static approximation is valid and one can use the effective permittivity model for multi-phase mixtures (Sihvola & Kong 1988). In the case of sand dunes, the thin laminations are characterized by changes of granulometry. In the following, we attempt to compute the effective permittivity that depends on the volumetric fraction of each sub-material in the mixture. For example, a dry sand is a mix of air and quartz grains with relative permittivities of $\kappa_0 = 1$ and $\kappa_q = 5$, respectively. If one considers a material containing spherical grains of homogeneous size (only one grain size), the more appropriate model is the Maxwell-Garnett (MG) formula (Maxwell-Garnett 1904) which is given by:

$$\kappa^* = \kappa_0 + 3(1-\phi)\kappa_0 \left[\frac{\kappa_q - \kappa_0}{\kappa_q + 2\kappa_0 - (1-\phi)(\kappa_q - \kappa_0)} \right]. \quad (1)$$

On the other hand, if the material is constituted by grains with an infinite number of sizes, that is to say a non-homogeneous grain size distribution, one can use the model described by the Hanai-Bruggeman–Sen (HBS) formula given for a mix of spherical grains and air (Bruggeman 1935; Hanai 1968; Sen *et al.* 1981):

$$\left[\frac{\kappa_q - \kappa^*}{\kappa_q - \kappa_0} \right] \left[\frac{\kappa_0}{\kappa^*} \right]^{1/3} = \phi. \quad (2)$$

In these formulas, the parameter ϕ is the porosity of the rocks which characterises the volumetric fraction of each component. In reality, however, rocks exhibit neither a single nor an infinite number of grain size. Therefore, these two models should form the limits which might border the observed data. In order to predict the permittivity of materials with a finite number of sizes, one can use the Robinson-Friedman (RF) recurrence formula given for a mix of

several grain sizes (Robinson & Friedman 2001):

$$\kappa_n = \kappa_{n-1} + 3\kappa_{n-1} \frac{\frac{f_n}{n}}{\phi + \sum_{n=1}^{} f_n} \cdot \frac{(\kappa_q - \kappa_{n-1})}{\kappa_q + 2\kappa_{n-1} - \frac{\frac{f_n}{n}}{\phi + \sum_{n=1}^{} f_n}(\kappa_q - \kappa_{n-1})}. \quad (3)$$

The number f_n is the volumetric fraction of the grains of size 'n' and has to validate the condition:

$$\sum_{n=1}^{N} f_n = 1 - \phi, \quad (4)$$

where N is the total number of sizes. Eq. (3) might be interpreted as an implementation of the MG model. It has already been studied experimentally with several mixes of glass beads (Robinson & Friedman 2001, 2005).

Usually, the grain size distribution is measured in terms of percentage of weight. In our study, we assume that the sand is composed exclusively of quartz of the same density. This allows us to consider the percentage of weight as being equivalent to the percentage of solid volume. In eq. (3), the volumetric fraction f_n of solid is related to the grain size distribution A_n and the porosity ϕ by the following equation:

$$f_n = (1-\phi)\frac{A_n}{\sum_{1}^{N} A_n}, \quad (5)$$

In Fig. 1, we show the implementation of eq. (3) for three different synthetic granulometry (grain size distribution A_n) data indicated by D1, D2 and D3, respectively. We take a range of grain sizes between 0.04 and 1 mm. As expected, in the case of a homogeneous
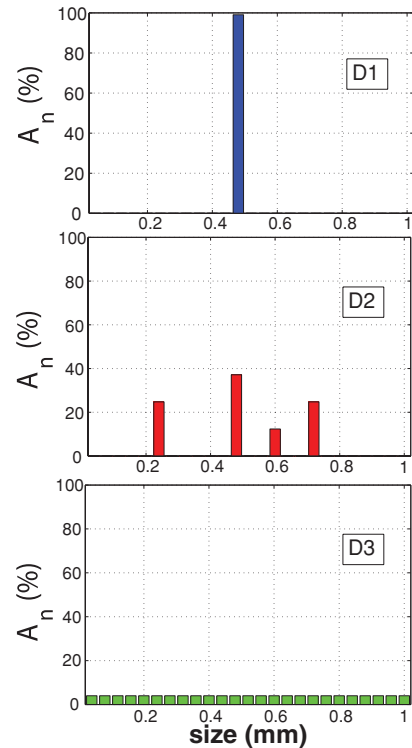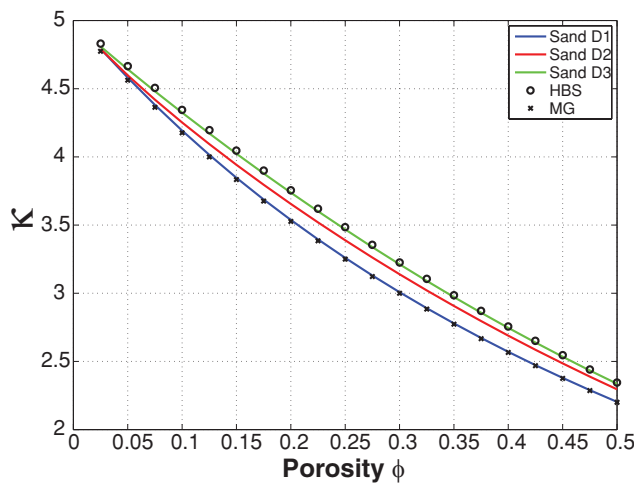
Figure 1. Influence of the granulometry (grain size distribution A_n) on permittivity model. The permittivity is plotted for a mix of quartz ($\kappa_q = 5$) and air ($\kappa_0 = 1$). D1: one size of 0.48 mm. D2: four sizes of 0.24, 0.48, 0.6 and 0.72 mm, respectively, D3: 25 sizes in the range of 0.04–1 mm).

distribution (D1: only one size of 0.48 mm) the result (blue line) fits with the MG model (eq. 1). If we consider a non-homogeneous distribution (D3: 25 sizes in the range of 0.04–1 mm), the result (green line) tends towards the HBS model (eq. 2), while in the intermediate case (D2: four sizes of 0.24, 0.48, 0.6 and 0.72 mm, respectively) the result (red line) is bounded by the two previous cases. These observations are in agreement with the fact that dry sand permittivity should be located between the two extreme cases which are described by the MG and HBS models, respectively.

For a constant porosity, the RF model (eq. 3) predicts a change of permittivity caused by the granulometry. Although this change is quite small, it might cause significant changes to the reflectivity of radar waves if we consider materials having small permittivity values, as is the case in dry sand dunes. However, some studies have shown that the grain size distribution controls the porosity as well. Therefore one has to bear in mind that the two parameters f_n and ϕ are joined (interfere with each other).

INFLUENCE OF THE GRANULOMETRY ON THE POROSITY

It is very difficult to use the granulometry to predict the porosity of a mix with more than two sizes. Indeed, while there is an analytical model that considers a bimodal mix of spheres (McGeary 1961; Marion *et al.* 1992), it cannot be accurately adapted to rocks because the shape of their components is not totally spherical. In this part, we present the 'fractional packing model' introduced by Koltermann & Gorelick (1995). This model is a semi-empirical law that gives the porosity of a bimodal mix. Let us consider a bimodal material composed of two parts: a 'small grain' and a 'large grain' that are characterised by their porosity ϕ_{small} and ϕ_{large}, respectively.

Each phase has a volumetric fraction F that satisfies the following condition:

$$F_{\text{small}} + F_{\text{large}} = 1. \tag{6}$$

It is important to note that F is different from the volumetric fraction of solid f_n introduced in the RF model. Indeed, the sum of the f_n has to fulfil the condition:

$$f_{\text{small}} + f_{\text{large}} = 1 - \phi_{\text{mix}}, \tag{7}$$

where ϕ_{mix} is the porosity of the mixture. The volumetric fraction of the solid f_n and the one of the phase F are related for each part by the equation:

$$f_{\text{small}} = (1 - \phi_{\text{small}})F_{\text{small}}. \tag{8}$$

The same relation is valid for the 'large grain' part. The 'fractional packing model' is separated in two regimes which correspond to different packing properties: (i) the coarse packing where fine grains are disposed inside the pore space of coarse grains (first part of the curve in Fig. 2), and (ii) the fine packing (second part of the curve in Fig. 2) where coarse grains are disposed inside a fine grain matrix. All of these cases are described in Fig. 2. This model depends on an empirical parameter, which is related to the ratio between the two sizes. In this paper we present only the resulting porosity for several ratios between two grain sizes ($R_{\text{large}}/R_{\text{small}} = 5$; 10 and 20, respectively). In Fig. 2, the fractional packing model is plotted for different ratio of sizes using a porosity of 0.48 which is in good agreement with values found in the literature for sand dunes (Atkins & McBride 1992). One can see that the bigger the size ratio ($R_{\text{large}}/R_{\text{small}}$), the lower the corresponding porosity value. The minimum porosity occurs when the volumetric fraction of the 'small grain' part is equal to the porosity of the 'large grain' part. This case corresponds to the central part of Fig. 2.
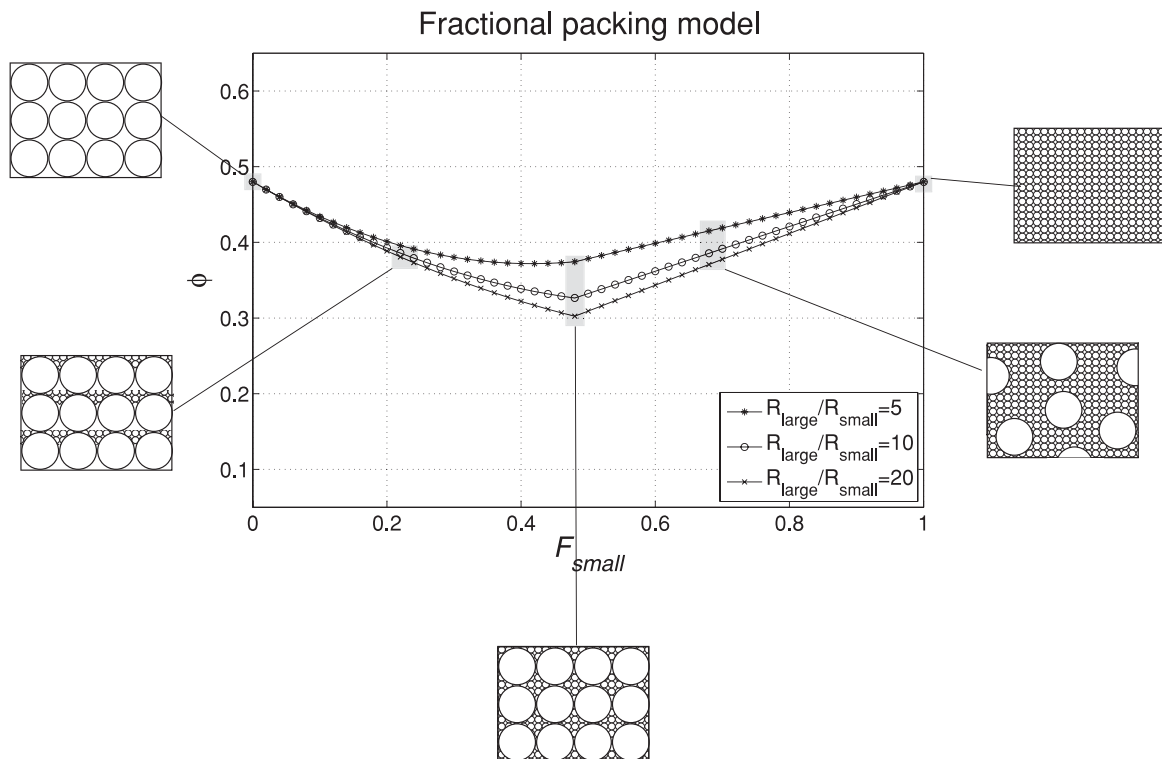
Figure 2. Fractional packing model introduced by Koltermann & Gorelick (1995). The porosity of each phase is taken to be equal to 0.48. The minimum of porosity corresponds to the case $F_{\text{small}} = \phi_{\text{large}}$.
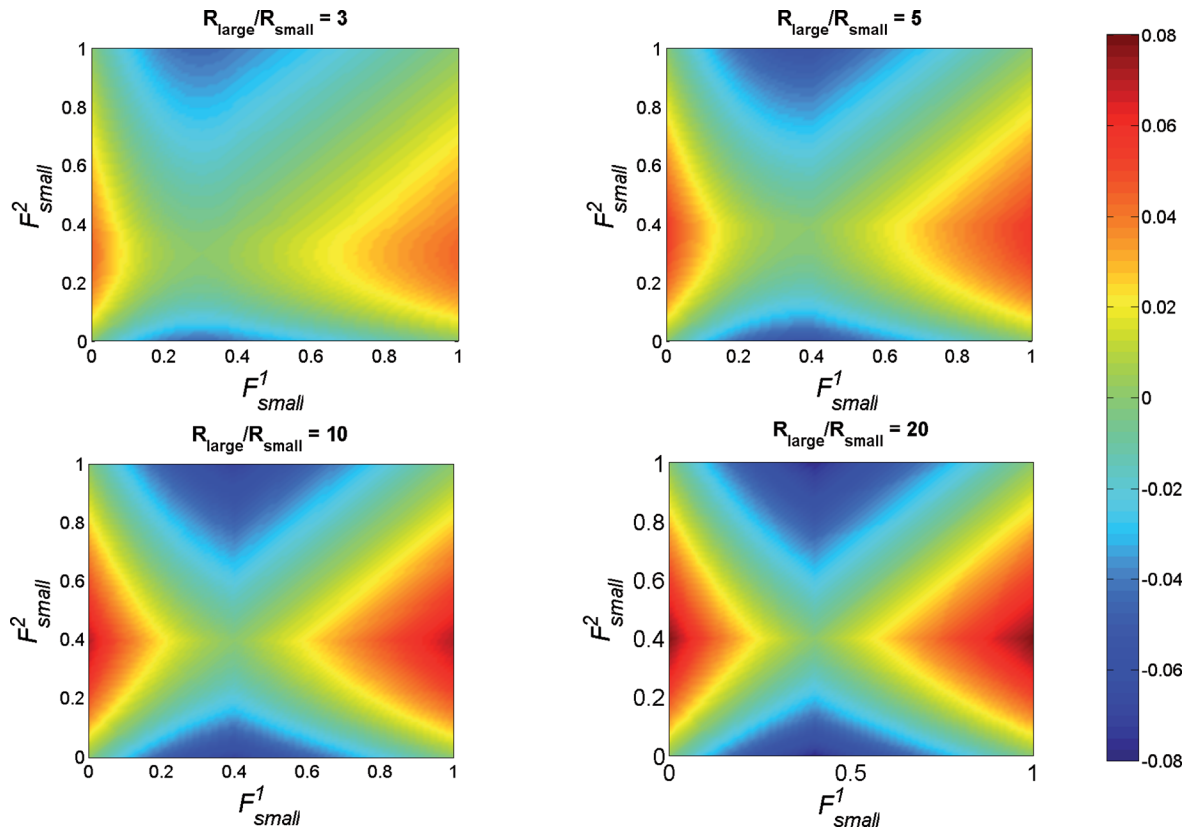
Figure 3. Theoretical reflectivity between two sandy horizontal layers with different grain size distribution. The strongest reflectivity occurs where there is contact between a well-sorted sand ($F_{small} \approx 0$ or 1) and a bimodal mix ($F_{small} \approx \phi_{large}$).

So far we have seen that the permittivity depends directly on the granulometry, as it is shown in the previous section. On the other hand, the granulometry indirectly influences the permittivity by controlling the porosity, as discussed in the present section. Therefore, in order to predict the permittivity of dry sand, we have to take into account not only the size distribution but also the porosity. Both of these parameters are related and are controlled by each other. In our study, we model the permittivity of effective bimodal sand using eq. (3) where the porosity is estimated by the fractional packing model.

Fig. 3 shows the GPR reflection coefficient for four different size ratios ($R_{large}/R_{small} = 3$; 5; 10 and 20, respectively). The results of Fig. 3 are computed with eq. (12) for a contact between two bimodal sands with volumetric fraction of the 'small grain' part F^1_{small} and F^2_{small} for a normally incident wave. The results indicate that, in some cases, the reflectivity can reach 8 per cent. One will notice that the higher the size ratio, the stronger the reflection coefficient. However, this only occurs where there is a strong change of grain size distribution which is the case of contact between well-sorted sand (only one grain size: where the part F of one of the two sizes is equal to 0 or 1) and bimodal sand ($F_{small} \approx \phi_{large}$).

INFLUENCE OF GRAIN SHAPE ON THE PERMITTIVITY

Changes in grain shape influence the level of connectivity of the material and influence the macroscopic electrical properties (Jackson *et al.* 1978; Sen *et al.* 1981). The eqs (1) and (2) are only valid for spherical grain. However, these laws can be generalized for all elliptic shapes by introducing a factor L depending on the

shape of the grains. In this context, the MG formula can be written as follows (Stratton 1941):

$$\kappa^* = \kappa_0 \left[\frac{\kappa_0 + (\kappa_q - \kappa_0)(1 - \phi + \phi L)}{\kappa_0 + L\phi(\kappa_q - \kappa_0)} \right], \tag{9}$$
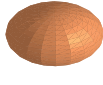
and the HBS model as follows (Sen *et al.* 1981; Greaves *et al.* 1996):

$$\left[\frac{\kappa_q - \kappa^*}{\kappa_q - \kappa_0} \right] \left[\frac{\kappa_0}{\kappa^*} \right]^L = \phi. \tag{10}$$

The parameter L is called the depolarization factor. It depends on the three elliptical radiuses (Mendelson & Cohen 1982; Boyle 1985; Asami 2002). Non-spherical grain yields to macroscopic anisotropy. Theoretically, L is a vector composed of three components with values between 0 and 1; the sum of these values is equal to unity. Each component corresponds to one direction of anisotropy. In our study, since we deal with 1D modelling for rays in the quasi-vertical direction (see below), we take L to be the scalar equivalent of the z-component of the anisotropic depolarizing factor. The values of L for different kinds of grain shape are presented in Table 1. By using these characteristics, one can model sand by mixing a set of spherical grains ($L = 1/3$) and a sandstone by mixing only a set of oblate spheres ($L = 0.5$) as it is suggested in Jackson *et al.* (1978) and Greaves *et al.* (1996). Introducing $L = 1/3$ in eq. (9) one can easily find the MG formula given in (1) for a well-sorted sand (containing identical spherical grains).

Table 1. Depolarizing factor for different grain shape.

Shape	Name	Axes	Depolarizing factor
	Cylinder	$a = b \ll c$	$L = 0$
	Sphere 'prolate'	$a = b < c$	$0 < L < 1/3$
	Sphere	$a = b = c$	$L = 1/3$
	Sphere 'oblate'	$a = b > c$	$1/3 < L < 1$
	Disk	$a = b \gg c$	$L = 1$

1D WAVELET MODELLING AND COMPARISON WITH REAL GPR DATA

The propagation and the reflection of the radar wave are calculated using the 1D wavelet modelling in the Fourier domain. This method, discussed by Bano (1996, 2004), gives the complex spectrum of a normally incident wavelet travelling through a homogeneous absorbing layer from $z = 0$ and reflected at a depth z as follows:

$$\vec{E}(z, \omega) = G(z) R_{12} \vec{E}(0, \omega) e^{i\omega\tau} e^{-\alpha 2z}, \tag{11}$$

where $\tau = 2z/V$ is the two way propagation time, V is the propagation velocity of EM waves, R_{12} is the reflection coefficient, $G(z)$ accounts for the geometrical spreading while $\vec{E}(0, \omega)$ is the complex spectrum of the electrical source of radar data at $z = 0$. The first exponential function models the propagation, and the second one considers the amplitude term related to the attenuation properties of the media. In our case, we consider a non-dispersive and non-attenuating medium ($\alpha = 0$). This is a good assumption for a material composed of dry sand, as it is the case of the dry dunes in the Chadian desert (see below).

The reflection coefficient R_{12} of a wave propagating through a homogeneous media with permittivity κ_1 and normally reflected at the interface of a second layer with the permittivity κ_2 is given by the following formula:

$$R_{12} = \frac{\sqrt{\kappa_1} - \sqrt{\kappa_2}}{\sqrt{\kappa_1} + \sqrt{\kappa_2}}. \tag{12}$$

The GPR data shown in Fig. 4a were collected in a dry sand dune in the Chadian desert using shielded antennas of 450 MHz. The acquisition was on transverse electrical (TE) mode with constant offset of 0.25 m and the antennas were moved by steps of 0.125 m. The first events in Fig. 4 are the direct air waves followed immediately by the direct ground waves; these events are superimposed. In this study, we use the first event of each trace as a source wavelet for the modelling of the GPR reflections inside the dune. This choice is largely discussed and justified in Bano (2004). The undulating reflection indicated by white arrows in Fig. 4a shows the base of the dune (which in fact is flat, see migration section in Fig. 4b and consists of pebbles (over 2.0 mm in diameter). This reflection is from the contact between the aeolian sands and the deeper lake deposits that consist of an unconsolidated silty sandstone layer of very fine to medium grain size. In Fig. 4a, we observe a nice diffraction hyper-

bola situated just under the base of the dune (see green circle), which fits very well with a velocity of 0.18 m/ns. This value represents a sort of average velocity from the top of the dune to the diffraction point and is in good agreement with values found in literature for dry sand (Von Hippel 1954; Costas *et al.* 2006; Gómez-Ortiz *et al.* 2009). The wavelength for the dominant frequency of 450 MHz and velocity $V = 0.18$ m/ns is 40 cm ($\lambda/4 = 10$ cm). This value is much larger than the grain size (from 0.02 to 2 mm diameter) and thin laminations inside the dunes.

In Fig. 4b we present the topographic Kirchhoff migration as it is discussed in Lehmann & Green (2000). The velocity used is constant and equal to 0.18 m/ns corresponding to an average permittivity of 2.8 for dry sand. A schematic interpretation of the migrated section is shown in Fig. 4c. The dune exhibits a complex internal structure with numerous bounding surfaces and it is composed of a minimum of four smaller dunes (indicated by 1, 2, 3 and 4, respectively, in Fig. 4c). From this figure, we can identify three kinds of reflectors:

- The ones which show a dip angle inside these small dunes (blue lines).
- The ones which may describe the surface of the internal small dunes (yellow lines).
- The reflector at the base of the system which is related to the contact between the sand and the bedrocks (brown line).

The first family of reflectors takes place within small dunes and is characterized by a large dip angle (between 15° and 25°). Some of these reflectors are shown in blue in Fig. 4c. Otto (1938) and Bagnold (1941) suggested that these internal laminations are probably related to the fluctuation of transporting power which may segregate grain size differently over time. Moreover, these aeolian deposits may alternate with avalanching (Hunter 1977, Mountney & Howell 2000).

If we consider the second family of reflectors (related to the old surfaces of dunes) and according to the observations of Bayard (1947) in Mauritania, the sand at the surface of dunes is compacted by the wind over few centimeters. Hunter (1977) defined these reflectors as the 'wind ripple surface', while Mountney & Howell (2000) observed a bimodal grain size distribution. As a consequence, the packing properties (for example the porosity ϕ) of this sand should differ from the sand inside the dune which may result, at least partly, from wind deposition and avalanching of the leeward slope.

Finally, the third kind of reflector is the bottom of the dune, which indicates the contact between aeolian sand and sandstone (see the brown line of Fig. 4c). The reflection coming from this latter reflector seems to be relatively strong (see the white arrows in Fig. 4a), which justifies our choice of a non-absorbing media and the consequential low probability of having water saturation inside the dune.

In the following analysis we model the radar reflections generated by these three reflectors. On the other hand, owing to the high velocity of the sand ($V = 0.18$ m/ns) and according to Annan *et al.* (1975) and Jiao *et al.* (2000), for an antenna located on the air–sand interface, the TE mode radiation has the largest amplitude at the critical angle $\theta_c = \sin^{-1}(V/0.3) = 37°$. Under this condition, the radiation pattern of the antenna is almost unchanged for angles between 0 and 25 degrees. Since we deal with 1D modelling for layers having a dip-angle between 0° and 25° (or for rays which deviate from the vertical on the range of 0–25°), the radiation pattern variation is not accounted for in eq. (11).

Thus, the spectrum of a wavelet reflected from a reflector inside the dune is calculated by using eq. (11), with the reflection
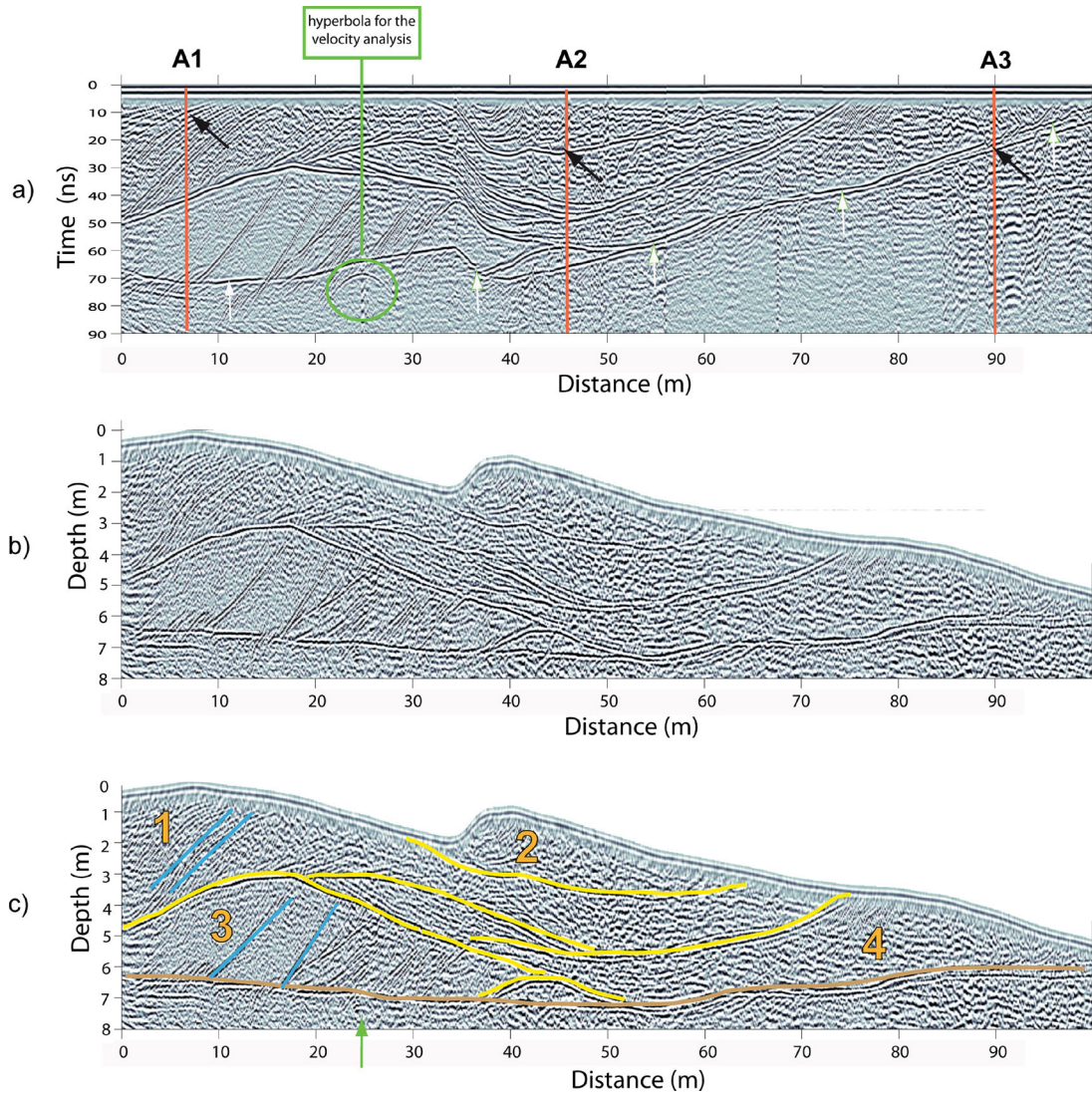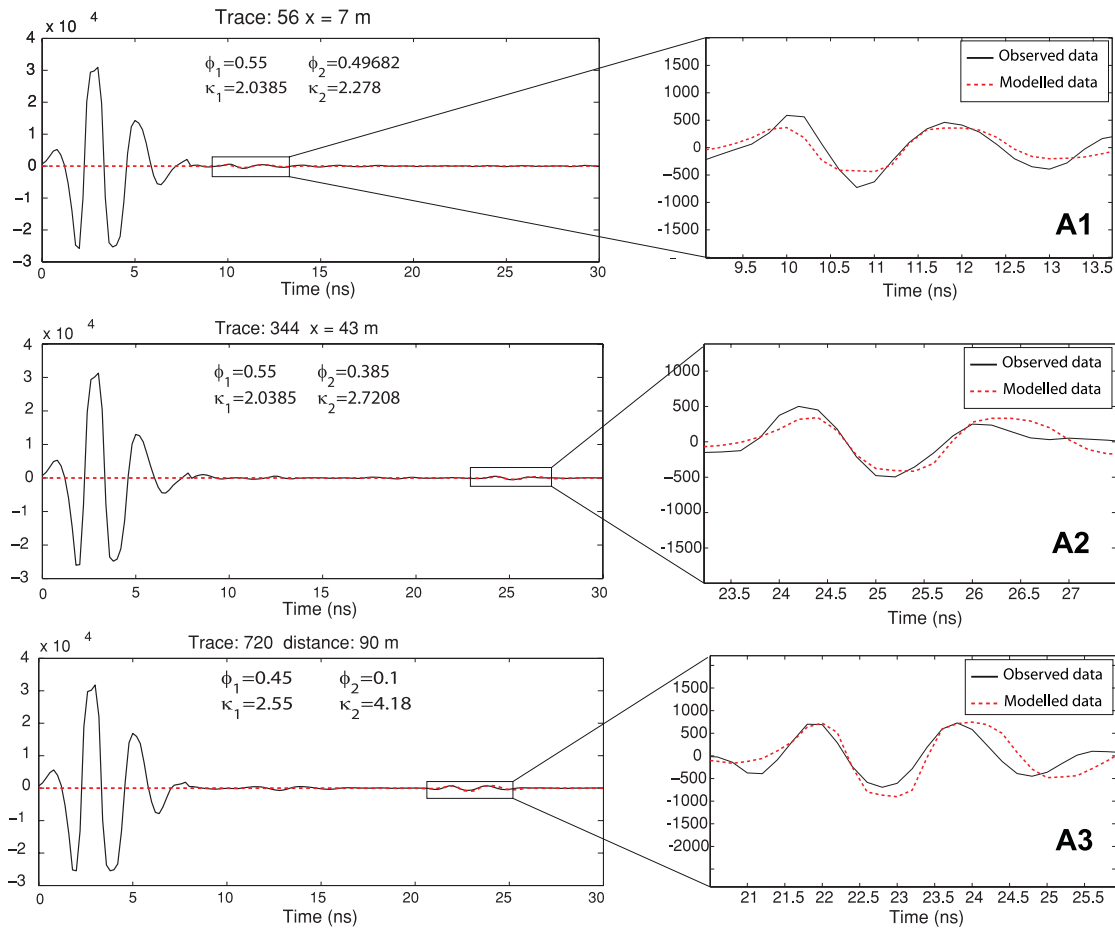
Figure 4. (a) The GPR section collected in a dry sand dune in the Chadian desert using shielded antennas of 450 MHz. The three vertical red lines refer to the traces, which are modelled in this paper. (b) The topographic Kirchhoff migration using a constant velocity of 0.18 m/ns. (c) Interpretation considering three kinds of bounding surface. Blue: change in granulometry. Yellow: change in compaction. Brown: contact sand/sandstone.

coefficient given by (12). The permittivities of the two layers (in eq. 12) are estimated by using the eqs (3) and (5), while the porosity ϕ is predicted by using the empirical modelling of Koltermann & Gorelick (1995). Although the traveltime τ (in eq. 11) can be read directly from the radar sections, we adjust it by minimizing the difference between the theoretical and real wavelets within a reasonable time interval. Afterwards, the theoretical reflected wavelet in time (obtained by transforming back the spectrum given in 11) is compared with the observed reflections.

The three observed reflections A1, A2 and A3 indicated by black arrows in Fig. 4 are supposed to be related to the three families of reflectors previously discussed. The comparisons of synthetic reflected wavelets (dashed lines) with three different real observed wavelets (A1, A2 and A3 in black) are shown in Fig. 5. The observed wavelet A1 (top) is compared to the theoretical GPR response (dashed line) that is supposed to be reflected from contact between mono-modal sand and a mixing of two sands with size ratio of 2. Here we note that this structural change, which is characterized by a small contrast of permittivity (2/2.25), causes a significant

reflectivity. The observed wavelet A2 (middle) is compared to the theoretical wavelet calculated for a contact between un-compacted well-sorted sand (one grain size) with porosity $\phi = 0.55$ and compacted bimodal sand with the total porosity $\phi = 0.39$. The comparison between the observed wavelet A3 and the synthetic wavelet is shown on the bottom of Fig. 5. The permittivities are computed using the HBS formula (10). The synthetic wavelet is calculated for a contact between dry sand ($\phi = 0.45$ and $L = 1/3$) and sandstone which corresponds to the reflection from the base of the dune. A good fit is found by considering a sandstone composed of oblate grains ($L = 0.5$ in eq. 10) with porosity $\phi = 0.1$. The effective permittivities (κ_1 and κ_2) of the two layers are shown within each graphic. They vary from 2 to 3 for the dune to 4.2 for the sandstone and are in good agreement with the values given by Davis & Annan (1989). It is interesting to notice that the value of permittivity for the dry sand estimated here is in good accordance with the value found by performing migration analysis of the diffraction hyperbola presented in Fig. 4a. Remember that the best migration velocity is equal to 0.18 m/ns which corresponds to a permittivity of 2.8 for dry sand.

Figure 5. Comparison between modelled (dashed line) and observed (solid line) GPR data for the three kinds of physical change presented in this study: size distribution (top), compaction (middle) and sand/sandstone contact (bottom). The wavelets presented are located at $x = 12$ m, $x = 43$ m and $x = 90$ m on the section shown in Fig. 4a.
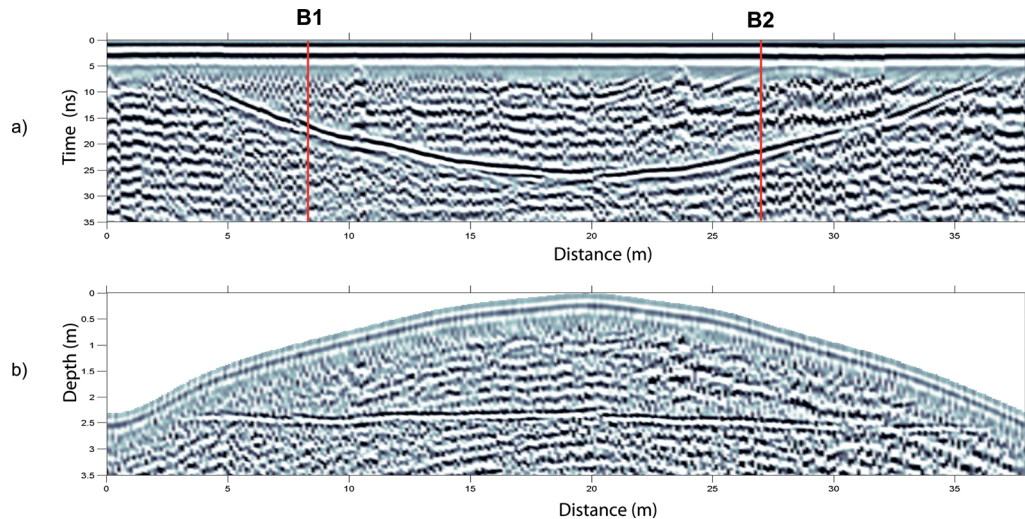

Figure 6. (a) The GPR section collected in a dry small dune using shielded antennas of 450 MHz. (b) The topographic Kirchhoff migration using a constant velocity of 0.18 m/ns. The two vertical red lines refer to the traces which are modelled in this paper.

Fig. 6a shows a second example of GPR data collected from a dry small dune using shielded antennas of 450 MHz. The bent reflection visible in this figure becomes a flat reflector after topographic migration with a velocity of 0.18 m/ns (see Fig. 6b). This reflector indicates the contact between the dry sand and sandstone

and corresponds to the base of the dune. To model the reflections from the bottom of the dune, the permittivities of the two layers are estimated by using eq. (10). We take $L = 0.33$ for the first layer (dry sand composed of spherical grains) and $L = 0.5$ for the second layer (sandstone composed of oblate grains). Two observed wavelets (B1
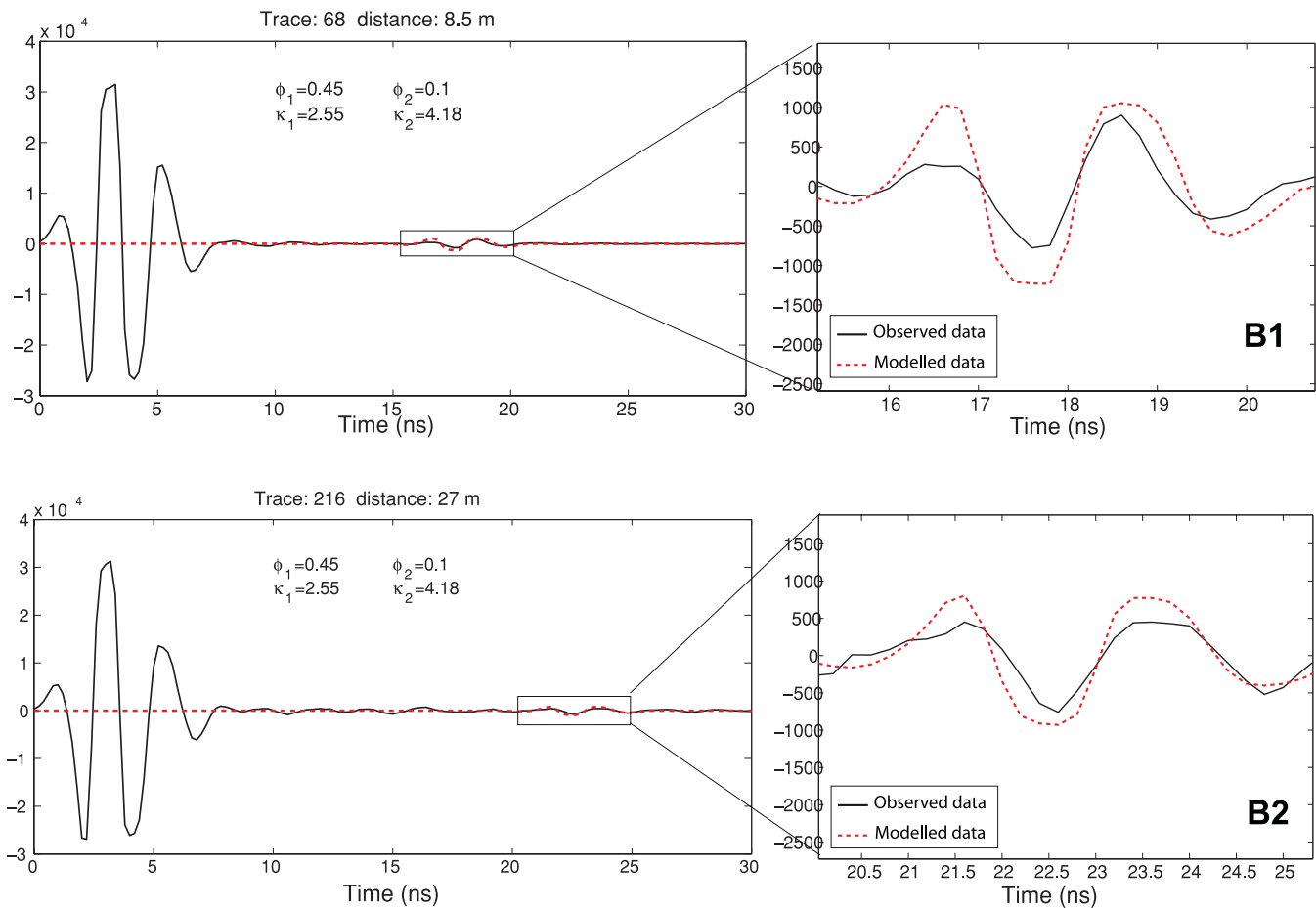
Figure 7. Comparison between modelled (dashed line) and observed (solid line) GPR data for sand/sandstone contact. The wavelets are located at $x = 8.5$ m and $x = 27$ m on the section shown in Fig. 6.

and B2 located to the traces indicated by vertical red lines in Fig. 6a) are compared with calculated wavelets and the results are shown in Fig. 7. The porosity of the sand is taken equal to 0.45 and a reasonable fit between the modelled and measured wavelets is found for a porosity of 0.1 for the sandstone.

CONCLUSION

In this study, we show that changes in grain size distribution, packing or grain shape are able to cause contrast in dielectric permittivity that is detectable by GPR. In order to predict the effective permittivity of dry sand, we use three MG, HBS and RF relationships, respectively. Using reasonable geological hypothesis about the properties of sand, we can use GPR modelling to explain the different boundaries encountered within dunes. We assume that the inclined reflectors are due to changes of grain size distribution resulting from the variation of wind depositions. We incorporate granulometry data in the effective permittivity formulas for a mixture of perfect spheres. By this way, we model an average granulometry of the thin laminations (due to high frequency alternating wind power) which are not detectable by GPR reflectivity. If we know precisely the permittivity of each small lamination (which depends on its granulometry), another way to estimate the effective permittivity, would have been to consider the effective medium as a mix of N thin plates ($L = 1$ in eq. 10) of sand with volumetric fraction of each lamination proportional to its thickness. On the other hand, we associate the big reflectors, which characterizes small internal dunes, to bimodal sand compacted by

the wind ('wind ripple surface'). Finally, we show that the largest contrast of permittivity corresponds to the base of the dune. We model it as the contact between sand and sandstone by using the HBS formula.

The results of the modelling show good accordance with GPR data obtained over two different dunes in the Chadian desert. However, the information contained in GPR data does not allow inverting the parameters of sands directly (due to equivalent models) without additional a priori information. In this paper we only show that it is possible to explain the observed GPR data by using a forward modelling that takes into account grain size distribution, packing and/or grain shape. Combining the application of the proposed method with additional constraining information from cores or trenches is the next logical step.

REFERENCES

Adetunji, A.Q., Al-Shuhail, A. & Korvin, G., 2008. Mapping the internal structure of sand dunes with GPR: a case history from the Jafurah sand sea of eastern Saudi Arabia, *Leading Edge,* **27,** 1446–1452.

Annan, A.P., Waller, W.M., Strangway, D.W., Rossiter, J.R., Redman, J.D. & Watts, R.D., 1975. The electromagnetic response of a low-loss, 2-layer, dielectric earth for horizontal electric dipole excitation, *Geophysics,* **40,** 285–298.

Asami, K., 2002. Characterization of heterogeneous systems by dielectric spectroscopy, *Prog. Polym. Sci.,* **27,** 1617–1659.

Atkins, J.E. & McBride, E.F., 1992. Porosity and packing of Holocene river, dune, and beach sands, *AAGP bulletin,* **76,** 339–355.

Bagnold, R.A., 1941. *The Physics of Blown Sand and Desert Dunes,* Methuen, London, 265pp.

Bano, M., 1996. Constant dielectric losses of ground-penetrating radar wave, *Geophys. J. Int.,* **124,** 279–288.

Bano, M., 2004. Modelling of GPR waves for lossy media obeying a complex power law of frequency for dielectric permittivity, *Geophys. Prospect.,* **52,** 11–26.

Bano, M. & Girard, J.F., 2001. Radar reflections and water content estimation of Aeolian sand dune, *Geophys. Res. Lett.,* **28,** 3207–3210.

Barndorf-Nielsen, O., Dalsgaard, K., Halgreen, C., Kuhlman, H., Moller, J.T. & Schou, G., 1982. Variation in particle size distribution over a small dune, *Sedimentology,* **29,** 53–65.

Bayard, 1947. Aspect principaux et consistence des dunes (Mauritanie), *Bull. de l'IFAN,* tome IX(1–4), 1–17 (in French).

Boyle, M.H., 1985. The electrical properties of heterogeneous mixtures containing an oriented spheroidal dispersed phase, *Coil. Polym. Sci.,* **27,** 1617–1659.

Bristow, C.S., Bailey, S.D. & Lancaster, N., 2000. The sedimentary structure of linear sand dunes, *Nature,* **406,** 56–59.

Bristow, C.S., Lancaster, N. & Duller, G.A.T., 2005. Combining ground penetrating radar surveys and optical dating to determine dune migration in Namibia, *J. geol. Soc. Lond.,* **162,** 315–321.

Bristow, C.S., Pugh, J. & Goodall, T., 1996. Internal structure of Aeolian sand dunes in Abu Dhabi determined using ground penetrating radar, *Sedimentology,* **43,** 995–1003.

Bruggeman, D., 1935. Berechung verschiederner physikalisher konstanten von hetarogenen substanzen, *Ann. Phys. Lpz.,* **24,** 636–679.

Costas, S., Alejo, I., Rial, F., Lorenzo, H. & Nombela, M.A., 2006. Cyclical evolution of a modern transgressive sand barrier in Northwestern Spain elucidated by GPR and aerial photos, *J. Sediment. Res.,* **76,** 1077–1092.

Davis, J. & Annan, A., 1989. Ground-penetrating radar for high resolution mapping of soil and rock stratigraphy, *Geophys. Prospect.,* **37,** 531–551.

Gómez-Ortiz, D., Martín-Crespo, T., Rodríguez, I., Sánchez, M.J. & Montoya, I., 2009. The internal structure of modern barchan dunes of the Ebro River Delta (Spain) from ground penetrating radar, *J. Appl. Geophys.,* **68,** 159–170.

Greaves, R.J., Lesmes, D.P., Mo Lee, J. & Nafi Toksöz, M., 1996. Velocity variations and water content estimated from multi-offset, ground-penetrating radar, *Geophysics,* **61,** 683–695.

Hanai, T., 1968. Electrical properties of emulsion, in *Emulsion Science,* pp. 354–477, ed. Sherman, P., Academic Press, London.

Harari, Z., 1996. Ground-penetrating radar (GPR) for imaging stratigraphic features and groundwater in sand dunes, *J. Appl. Geophys.,* **36,** 43–52.

Hunter, R.E, 1977. Basic types of stratification in small eaolian dunes, *Sedimentology,* **2,** 361–387.

Jackson, P.D., Smith, D.T. & Stanford, P.N., 1978. Resistivity-porosity-particle shape relationships for marine sands, *Geophysics,* **43,** 1250–1268.

Jiao, Y., McMechan, G.A. & Pettinelli, E., 2000. In situ 2-D and 3-D measurements of radiation patterns of half-wave dipole GPR antennas, *J. Appl. Geophys.,* **43,** 69–89.

Jol, H.M., 1995. Ground penetrating radar antennae frequencies and transmitter powers compared for penetration depth, resolution and reflection continuity, *Geophys. Prospect.,* **43,** 693–709.

Koltermann, C. & Gorelick, S., 1995. Fractional packing model for hydraulic conductivity derived from sediment mixtures, *Water Resour. Res.,* **31,** 3283–3297.

Lancaster, N., 1989. *The Namib Sand Sea: Dunes Forms, Processes and Sediments,* AA Balkema, Rotherdam, 200pp.

Lehmann, F. & Green, A.G., 2000. Topographic migration of georadar data: implication for acquisition and processing, *Geophysics,* **65**(3), 836–848.

McGeary, R.K., 1961. Mechanical packing of spherical particles, *J. Am. Ceram. Soc.,* **44,** 513–522.

Marion, D., Nur, A., Yin, H. & Han, D., 1992. Compressional velocity and porosity in sand-clay mixtures, *Geophysics,* **57**(4), 554–563.

Maxwell-Garnett, J., 1904. Colours in metal glasses and metal films, *Philos. Trans. R. Soc. Lond.,* Sect. A, **3,** 385–420.

Mendelson, K.S. & Cohen, M.H., 1982. The effect of grain anisotropy on the electrical properties of sedimentary rocks, *Geophysics,* **47,** 257–263.

Mountney, N. & Howell, J., 2000. Aeolian architecture, bedform climbing and preservation space in the Cretaceous Etjo Formation, NW Namibia, *Sedimentology,* **47,** 825–849.

Neal, A. & Roberts, C.L., 2001. Internal structure of a through blowout determined from migrated ground-penetrating-radar profiles, *Sedimentology,* **48,** 791–810.

Otto, G.H., 1938. The sedimentation unit and its use in field sampling, *J. Geol.,* **46,** 569–582.

Robinson, D. & Friedman, S., 2001. Effect of particle size distribution on the effective dielectric permittivity of saturated granular media, *Water Resour. Res.,* **37,** 33–40.

Robinson, D. & Friedman, S., 2005. Electrical conductivity and dielectric permittivity of sphere packing: measurements and modelling of cubic lattices, randomly packed monosize spheres and multi-size mixtures, *Physica A,* **358,** 447–465.

Sen, P., Scala, C. & Cohen, M., 1981. A self-similar model for sedimentary rocks with application to dielectric constant of fused glass beads, *Geophysics,* **46,** 781–795.

Shenk, C.J, Gautier, D.L., Olhoeft, G.R & Lucius, J.E, 1993. Internal structure of an aeolian dune using ground-penetrating-radar, *Spec. Publs Ass. Sediment,* **16,** 61–69.

Sihvola, A.H. & Kong, J.A., 1988. Effective permittivity of dielectric mixtures, *IEEE Trans. Geosci. Remote Sens.,* **26,** 420–429.

Stratton, J.A., 1941. *Electromagnetic Theory,* pp. 213–214, McGraw-Hill Book Co. Inc, New York, NY.

Thomas, D.S.G., 1988. Analysis of linear dune sediment-form relationships in the Kalahari dune desert, *Earth Surface Processes Landforms,* **16,** 545–553.

Von Hippel, A.R., 1954. *Dielectric Materials and Applications,* Technology Press of M.I.T., New York, NY.

Wang, X., Dong, Z., Zhang, J., Qu, J. & Zhao, A., 2003. Grain size characteristics of dune sands in the central Taklimakan Sand Sea, *Sedimentary Geol.,* **161,** 1–14.

Watson, A., 1986. Grain size variations on a longitudinal dune and a barchan dune, *Sedimentary Geol.,* **46,** 49–66.

Widess, M.B., 1973. How thin is a thin bed?, *Geophysics,* **38,** 1176–1180.

Zeng, H., 2009. How thin is a thin bed? An alternative perspective, *Leading Edge,* October, 1192–1137.